Mechanics of Advanced Materials and Structures, 19:119–128, 2012

ISSN: 1537-6494 print / 1537-6532 online
DOI: 10.1080/15376494.2011.572242

Taylor & Francis
Taylor & Francis Group

Prediction of Micro and Nano Indentation Size Effects from Spherical Indenters

Rashid K. Abu Al-Rub and Abu N. M. Faruk
Zachry Department of Civil Engineering, Texas A&M University, College Station, Texas, USA

In the present work, a micromechanical model based on dislocation mechanics for predicting indentation size effect from spherical indenters is developed and compared with the most widely used Swadener et al. (2002) model. The key idea proposed here while deriving the model is that a nonlinear coupling between the geometrically necessary dislocations (GNDs) and the statistically necessary dislocations (SSDs) can largely correct the deviation of the Swadener et al. model's prediction from hardness results for small diameter indents. Furthermore, the model can be used in identifying the material length scale from micro- and nano-indentation data.

Keywords indentation size effect, micro-indentation, nano-indentation, geometrically necessary dislocations, statistically stored dislocations, length scale

1. INTRODUCTION

With the emerging area of nanotechnology in recent years, there has been a significant and rapidly growing effort to fabricate small structures in the micro- and nano-meter scales. Along with it came the challenge of evaluating the mechanical properties (e.g., hardness, stiffness, etc.) of materials at these small scales. Micro- and nano-indentation tests (i.e., typically indentation depths on the order of 0.1 to 100 micrometers and less than 0.1 micrometers, respectively) proved to be the most suitable for their economic as well as fast, precise, and nondestructive merit. However, there are numerous indentation tests at scales on the order of a micron or a submicron that have shown that the measured hardness increases significantly with decreasing the indentation size or equivalently the indenter size (e.g., [1–9]). This phenomenon is commonly referred to as the indentation size effect (ISE).

There are several examples of size effects other than ISE. For example, experimental work has revealed that a substantial increase in the macroscopic flow stress can be achieved by decreasing the particle size of particle-reinforced composites while keeping the volume fraction constant (e.g., [10–12]), and with decreasing the thickness of thin films in micro-bending test (e.g., [13–15]). None of these cases of dependence of mechanical response on size could be explained by the classical continuum mechanics whereas the gradient plasticity theory has been successful in addressing the size effect phenomena (see the book by Voyiadjis and Abu Al-Rub [16] for a detailed review of gradient plasticity theory). This is due to the incorporation of a micro-structural length scale parameter in the governing equation of the deformation description. Gradient plasticity theory attributes ISE to the evolution of the so-called geometrically necessary dislocations (GNDs) beneath the indenter, which gives rise to strain gradients [17, 18].

By considering the GNDs generated by a conical indenter, Nix and Gao [19] utilized the dislocation arguments set by Stelmashenko et al. [1] and Ma and Clarke [3] and developed an ISE model that suggests a linear dependence of the square of the micro-hardness to the inverse of the indentation depth. Swadener et al. [9] utilized the basic precepts given by Nix and Gao [19] for a conical indenter and developed an ISE model for spherical indenters which suggests a linear dependence of the square of the micro-hardness to the inverse of the diameter of the spherical indenter. However, recent micro- and nano-indentation results show that the predictions of the Nix-Gao and Swadener et al. models deviate significantly from the experimental results at small indentation depths (i.e., nano-indentation) in the case of Berkovich and Vickers indenters (e.g., [6, 7, 20–26]) and at small diameters for the case of spherical indenters [9, 22]. Moreover, Elmustafa and Stone [7] observed that when the Nix-Gao model is used to fit the experimental results of micro- and nano-hardness, the data at deep indents (micro-hardness) exhibits a straight-line behavior whereas for shallow indents (nano-hardness) the slope of the line severely changes, decreasing by a factor of 10, resulting in a bilinear behavior and, therefore, two different values for the material length scale are used to fit the micro- and nano-indentation data. Recently, Huang et al. [27] modified the Nix-Gao model by reducing the density of GNDs at small indentation depths where two values for the

Received 16 August 2009; accepted 13 April 2010.
Address correspondence to Rashid K. Abu Al-Rub, Zachry Department of Civil Engineering, 710B CE/TTI Building, 3136 TAMU, College Station, TX 77843, USA. E-mail: rabualrub@civil.tamu.edu

material length scale are also used to fit the micro- and nano-indentation data. Chicot [28] has shown that the Nix-Gao model is able to represent micro- and nano-indentation results if the dislocation spacing under the conical indenter is considered non-uniform and the plastic volume size is assumed to be higher in nano-indentation compared to micro-indentation as confirmed by Durst et al. [29]. Two material length scales are used to fit the experimental data. Therefore, Nix-Gao model can fit well either the hardness data from micro-indentation or nano-indentation tests, but not both simultaneously. The same can be said about Swadener et al. [9] ISE model for spherical indenters.

Recently, Abu Al-Rub [25] and Abu Al-Rub and Faruk [26] argued that the most likely impediment in the Nix and Gao [19] ISE model is the assumption that the densities of GNDs and SSDs in the Taylor's hardening law [30] are summed arithmetically such that it underestimates the total dislocation density underneath a conical/pyramidal indenter. It was concluded that it is better to postulate the total shear stress as the arithmetic sum of the shear stresses from SSDs and that from GNDs. Therefore, this conclusion is used here in order to formulate a new ISE model for spherical indenters as compared to that by Swadener et al. [9]. Moreover, the present study shed some insight on the interpretation of the ISE encountered in micro- and nano-hardness from spherical indenters and proposes an ISE analytical model that can predict equivalently well the micro- and nano-indentation hardness data from spherical indentation. The predictions of this model are compared to that by Swadener et al. [9] against a set of micro-indentation tests on several metallic materials from the literature. Values for the material length scale parameter are calculated and it is shown that these values vary with the plastic strain for a certain material.

2. STRAIN GRADIENT PLASTICITY THEORY AND COUPLING BETWEEN SSDs AND GNDs

Plastic strain gradients play an essential role in the prediction of size-scale effects in the deformation behavior of metals at the micron and submicron scales. The classical plasticity theory, which inherently includes no material length scale, cannot predict size effects. Strain gradient plasticity theories extend the classical plasticity models by explicitly including an intrinsic material length scale and by including the history effects of the surrounding material points on the material point under consideration (i.e., nonlocality), and are therefore appropriate for materials and structural systems involving small dimensions. Many researchers tend to write the weak form of the non-local conventional effective plastic strain, $\widehat{\varepsilon}^p$, which is the conjugate variable of the plasticity isotropic hardening, in terms of its local counterpart, ε^p, and the corresponding higher-order gradients, η. The coupling between $\widehat{\varepsilon}^p$ and η was presented in many different mathematical forms by Abu Al-Rub and Voyiadjis [22, 31]. Motivated by the Taylor's hardening law at the micro-mechanical level, one can assume the following power-law of the corresponding gradient-dependent flow stress at the mesoscale [25]:

$$\sigma = \sigma_{ref}(\widehat{\varepsilon}^p)^{1/n} \quad \text{with} \quad \sqrt{\widehat{\varepsilon}^p} = \sqrt{\varepsilon^p} + \sqrt{\ell\eta}. \tag{1}$$

where σ can be set equal to the effective (or equivalent) stress, for example, $\sigma = \sqrt{3 s_{ij} s_{ij}/2}$ in case of von Mises-type plasticity, where $s_{ij} = \sigma_{ij} - \frac{1}{3}\sigma_{kk}\delta_{ij}$ is the deviatoric part of the Cauchy stress tensor σ_{ij} with δ_{ij} designates the Kronecker delta. The reference stress σ_{ref} is a measure of the yield strength in uniaxial tension, ℓ is the material length scale where its physical meaning and origin will be explored in the following developments, $n \geq 1$ is the strain-hardening exponent, and η is an effective measure of the gradient of plastic strain which is related to the GND density. For example, one can assume $\eta = \sqrt{\nabla\varepsilon^p . \nabla\varepsilon^p}$, where ∇ is the first-order gradient operator. For other expressions of η, one can consult Abu Al-Rub and Voyiadjis [22].

It is assumed, in general, that the total dislocation density represents the total coupling between two types of stored dislocations which play a significant role in the hardening mechanism of small scale metallic systems; namely: statistically stored dislocations (SSDs) and geometrically necessary dislocations (GNDs) [17, 18, 32]. SSDs are generated by trapping each other in a random way while GNDs relieve the plastic deformation incompatibilities within the polycrystal caused by non-uniform dislocation slip. GNDs cause additional storage of defects and increase the deformation resistance by acting as obstacles to SSDs. Furthermore, the density of SSDs, ρ_S, depends on the local effective plastic strain, ε^p, while the density of GNDs, ρ_G, is directly proportional to the gradient of the effective plastic strain, $\nabla\varepsilon^p$ [17]; thus, introducing nonlocality. The densities ρ_S and ρ_G can be combined in various ways for which, unfortunately, there is a little guidance from dislocation mechanics until now. Mughrabi [33] concluded that the simple superposition of the density of GNDs on the density of SSDs (i.e., $\rho_T = \rho_S + \rho_G$) is not well founded and they are unambiguously related. Abu Al-Rub and Voyiadjis [22, 31], Voyiadjis and Abu Al-Rub [34], and Abu Al-Rub [25] presented different phenomenological forms to enhance the nonlinear coupling between SSDs and GNDs. They have concluded that the most likely impediment in the Nix and Gao [19] model in predicting nano-hardness from conical/pyramidal indenters is due to the assumption that the total dislocation density, ρ_T, in the Taylor's hardening law is a simple arithmetic sum of both SSD and GND densities. One possible coupling can be assessed by writing the overall flow stress, σ, as follows:

$$\sigma = \left[\sigma_S^\beta + \sigma_G^\beta\right]^{1/\beta}, \tag{2}$$

where the interaction coefficient β is considered as a material constant and used to assess the sensitivity of predictions to the way in which the coupling between the SSDs and GNDs is enhanced during the plastic deformation process. The general

form in Eq. (2) ensures that $\sigma \to \sigma_S$ whenever $\sigma_S \gg \sigma_G$ (i.e., classical plasticity) and that $\sigma \to \sigma_G$ whenever $\sigma_S \ll \sigma_G$. The stresses σ_S and σ_G are associated, respectively, with the densities of SSDs and GNDs through the Taylor's hardening law [30] as follows:

$$\sigma_S = m\alpha Gb\sqrt{\rho_S}, \quad \sigma_G = m\alpha Gb\sqrt{\rho_G}, \tag{3}$$

where m is the Taylor's factor, which acts as an isotropic interpretation of the crystalline anisotropy at the continuum level such that $m = \sqrt{3}$ for an isotropic solid and $m = 3.08$ for FCC polycrystalline metals [30], G is the shear modulus, b is the magnitude of Burgers vector, and α is a statistical coefficient between 0.1 and 0.5.

Substituting Eqs. (3) into Eq. (2), one can express the total dislocation density, ρ_T, as follows:

$$\rho_T = \left[\rho_S^{\beta/2} + \rho_G^{\beta/2}\right]^{2/\beta}, \tag{4}$$

such that the flow stress σ in Eq. (2) can be rewritten as:

$$\sigma = m\alpha Gb\sqrt{\rho_T}. \tag{5}$$

However, recently, Abu Al-Rub [25] has shown that the real situation in experiments suggests that ρ_T cannot be taken as a simple sum of the densities of SSDs and GNDs (i.e., for $\beta = 2$) and that the total dislocation density under indentation is larger than this simple sum. In fact, for $\beta < 2$ in Eq. (4), ρ_T is larger than the arithmetic sum of SSD and GND densities, whereas for $\beta > 2$, ρ_T is smaller than the sum. Therefore, β either increases the effect of both kinds of dislocations or decreases such effect. However, Ashby [17] has pointed out that in general the presence of GNDs will accelerate the rate of SSDs storage and that an arithmetic sum of their densities gives a lower limit on ρ_T, which implies that β should be less than 2. In fact, Abu Al-Rub [25] has concluded after analyzing several micro- and nano-hardness data from indentation by conical/pyramidal indenters that $\beta \approx 1$ in Eq. (4). In other words, Abu Al-Rub [25] has concluded that a simple arithmetic sum of the flow stresses from the densities of SSDs and GNDs is a better assumption than the simple sum of the densities of SSDs and GNDs. Hence, by setting $\beta = 1$ in Eq. (2), one can rewrite the total flow stress as follows:

$$\sigma = \sigma_S + \sigma_G. \tag{6}$$

This along with Eq. (4) leads to a coupling between SSD and GND densities of the form,

$$\sqrt{\rho_T} = \sqrt{\rho_S} + \sqrt{\rho_G}. \tag{7}$$

Equation (7) gives a total dislocation density larger than that given by $\rho_T = \rho_S + \rho_G$. In the following subsequent developments, Eqs. (1), (3), and (6) will be utilized to formulate an ISE model and in exploring the physical origin of the material length scale parameter responsible for the observed size-scale effects.

3. PHYSICAL INTERPRETATION OF THE INTRINSIC MATERIAL LENGTH SCALE

The full utility of the strain gradient plasticity theories hinges on one's ability to determine the constitutive length scale parameter, ℓ, which scales the gradient effect. In this section, the physical intepretation of ℓ is identified.

During plastic deformation, the density of SSDs increases due to a wide range of processes that leads to production of new dislocations. Those new generated dislocations travel on a background of GNDs, which act as obstacles to the SSDs. If L_S is the average distance traveled by a newly generated dislocation, then the rate of accumulation of strain due to SSDs scales with $\dot{\varepsilon}^p \propto b\rho_S\dot{L}_S$ [35]. However, a more transparent assumption is $\dot{\varepsilon}^p \propto b\,\overline{\rho_S L_S}$ (where $\dot{\overline{\rho_S L_S}}\,\dot{L}_S\rho_S + L_S\dot{\rho}_S$) such that for proportional loading and monotonically increasing plasticity, one can express ε^p in terms of ρ_S as [22, 31]:

$$\varepsilon^p = \frac{1}{m} bL_S\rho_S. \tag{8}$$

On the other hand, Ashby [17] and Arsenlis and Parks [18] showed that gradients in the plastic strain field are accommodated by the GND density, ρ_G, such that the effective plastic strain gradient η that appears in Eq. $(1)_2$ can be defined as follows:

$$\eta = \frac{\rho_G\, b}{\bar{r}}. \tag{9}$$

The constant $\bar{r} \approx 2$ is the Nye's factor introduced by Arsenlis and Parks [18] to reflect the scalar measure of GND density resultant from mesoscopic plastic strain gradients.

Now, substituting ρ_S from Eq. (8) and ρ_G from Eq. (9) into Eq. (7) and then in Eq. (5), and comparing the result with Eq. $(1)_1$ after substituting Eq. $(1)_2$ yields the following expression for the intrinsic material length scale ℓ in term of the mean free path of dislocations or the mean spacing between dislocations, L_S, such that

$$\ell = \Gamma L_S \quad \text{with} \quad \Gamma = \bar{r}/m, \tag{10}$$

which also gives σ_{ref} as:

$$\sigma_{ref} = G\sqrt{\alpha^2 m^3 b/L_S}. \tag{11}$$

The micro-structural length scale parameter, ℓ, and the phenomenological measure of the yield stress in uniaxial tension, σ_{ref}, are now related to measurable physical parameters. It appears from Eq. $(10)_1$ that the size effect and its implications

on the flow stress and work-hardening in metals is fundamentally controlled by the dislocation glide, which depends on the course of deformation and the material's microstructural features. If one assumes $m \approx 2$ and $\bar{r} \approx 2$ then $\ell \approx L_S$, which can be experimentally measured. Therefore, L_S is a crucial physical measure that controls the evolution of the length scale in gradient plasticity theory for metals such that the key feature of plastic deformation is the reduction of the free path, cell size, or spacing between dislocations with deformation, material's microstructure, and size of the structural system.

By substituting L_S from Eq. $(10)_1$ into Eq. (11), one obtains a relation for ℓ as a function of the shear modulus, yield stress, and other micro-structural parameters, such that:

$$\ell = m^2\alpha^2\bar{r}(G/\sigma_{ref})^2 b. \tag{12}$$

This agrees with the expression proposed by Nix and Gao [19]. If one sets $m = 3.08$, $\alpha = 0.3$, $b = 0.225\,\text{nm}$, and $G/\sigma_{ref} = 100$, where those values are in the range of many pure metals, then $\ell = 3.8\,\mu\text{m}$, which is a physically sound value in the range of micrometers as reported by many authors in the Material Science community (e.g., [13, 19, 22, 31, 36, 37]).

4. ISE MODEL FOR THE SPHERICAL TIPPED INDENTERS

Let us consider the indentation by a rigid sphere, as shown in Figure 1. One can assume that the density of GNDs is integrated by the geometry of the indenter and the indentation is accommodated by circular loops of GNDs with Burgers vectors normal to the plane of the surface. The fundamental parameters for indentation tests by a spherical indenter are (see Figure 1): the force applied to the indenter, P, the residual contact radius of indentation, a_p, the hardness, $H = P/\pi a_p^2$, the permanent indentation depth, h_p, the total indentation depth, h, the residual indentation profile diameter, D_p, the plastic zone radius, c_p, which is scaled to a_p with a factor f such that $c_p = f a_p$, and the indenter geometry (i.e., the sphere diameter D). Due to the importance of the unloading process for the proper specification of these parameters, h_p and a_p should be used as measureable data in the hardness, H calculation as well as the residual indentation profile diameter $D_p > D$ when using a spherical indenter.

It can be assumed that the spherical indenter is approximated by a paraboloid and the indentation profile in the unloaded configuration can be described by:

$$w(r) = h_p - \frac{r^2}{D_p} \quad \text{for} \quad 0 \le r \le a_p, \tag{13}$$

where h_p, a_p, and D_p are measured in the unloaded configuration. By taking the slope of Eq. (13) and comparing it with

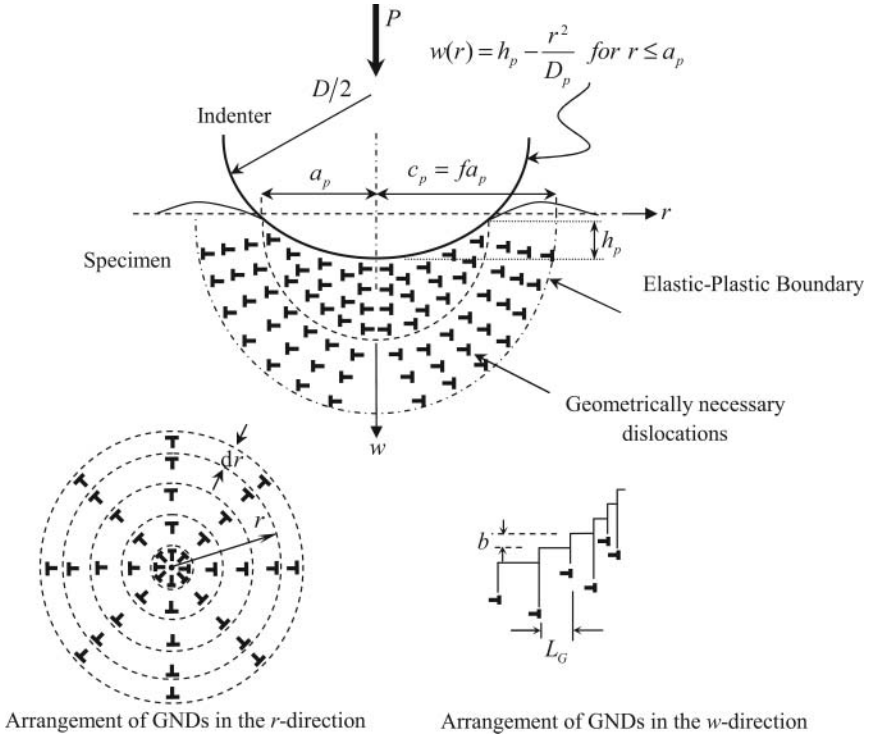

FIG. 1. Axisymmetric rigid spherical indenter. Geometrically necessary dislocations created during the indentation process. The dislocation structure is idealized as circular dislocation loops.

Figure 1, one can easily show that:

$$\left|\frac{dw}{dr}\right| = \frac{2r}{D_p} = \frac{b}{L_G} \Rightarrow L_G = \frac{bD_p}{2r}, \tag{14}$$

where L_G is the mean spacing between the individual slip steps on the indentation surface corresponding to the GND loops. One can conclude from Eq. (14) that the GND loops are more closely spaced as one move away from the center of the spherical indenter in order to accommodate the geometric shape of the indenter.

Moreover, it is assumed that the dislocation evolution during indentation is primarily governed by a large hemispherical volume V that scales with the contact radius a_p around the indentation profile (see Figure 1). However, the GNDs reside inside a plasticity zone, which can be viewed as extending to a radius c_p to the outermost dislocation emanated from the indent core. Therefore, the size of the plastic zone, c_p, underneath the indenter is larger than the contact radius, a_p, as suggested by Feng and Nix [21] and Durst et al. [29] such that $c_p = fa_p$ where $f > 1$.

Now, if λ is the total length of induced GND loops, then between r and $r + dr$ one has:

$$d\lambda = 2\pi r \frac{dr}{L_G} = 4\pi \frac{r^2}{bD_p} dr, \tag{15}$$

which upon integrating over the radius of the plastic volume V (i.e., $c_p = f\, a_p$) gives:

$$\lambda = \int_0^{c_p} \frac{4\pi}{bD_p} r^2 dr = \frac{4\pi f^3 a_p^3}{3bD_p}. \tag{16}$$

If one assumes that all the induced GND loops reside within the net volume V, which is calculated as the indentation volume ($\frac{1}{2}\pi a_p^2 h_p$) subtracted from the total hemispherical volume of radius c_p (i.e., $\frac{2}{3}\pi c_p^3$), such that:

$$V = \frac{2}{3}\pi\gamma f^3 a_p^3 \quad \text{with} \quad \gamma = 1 - \frac{3}{4f^3}\left(\frac{h_p}{a_p}\right). \tag{17}$$

Now, one can calculate the GNDs density using the following relation:

$$\rho_G = \frac{\lambda}{V} = \frac{2}{b\gamma D_p}, \tag{18}$$

which shows that the density of GNDs is proportional to the inverse of the diameter of the spherical indenter analogous to the proportionality to the indentation depth in Nix and Gao [19] model for pyramidal indenters.

Tabor [38] specified the mapping from the $H - h$ curve to $\sigma - \varepsilon^p$ curve such that one can assume the following mapping:

$$H = \kappa\sigma, \quad \varepsilon^p = c\omega, \tag{19}$$

where the parameter κ is the Tabor's factor, which has a value from 2.8 to 3.07, c is a material constant with a value of $c = 0.4$ [39] and $\omega = a_p/D_p$ defines the ratio between the contact radius to the indenter diameter in the unloaded configuration. The Tabor's relations in Eq. (19) has been extensively verified and used by many authors in the literature and, therefore, one may indeed take them as a starting point. Thus, one can define the micro/nano-hardness (i.e., size-dependent hardness), H, and macro-hardness (i.e., size-independent hardness), H_o, as follows:

$$H = \kappa m\alpha bG\left(\sqrt{\rho_S} + \sqrt{\rho_G}\right), \; H_o = \kappa m\alpha bG\sqrt{\rho_S}. \tag{20}$$

From the above equations, one can write the ratio of H/H_o as:

$$\frac{H}{H_o} = 1 + \sqrt{\frac{\rho_G}{\rho_S}}. \tag{21}$$

Considering Eqs. (8), (10), and $(19)_2$, yields the following expression for the density of SSDs:

$$\rho_s = \frac{c\bar{r}\omega}{\ell b}. \tag{22}$$

Substituting Eqs. (18) and (22) into (21), yields:

$$\frac{H}{H_0} = 1 + \sqrt{\frac{a^*}{a_p}}, \tag{23}$$

where

$$a^* = \varsigma\ell \quad \text{with} \quad \varsigma = \frac{2}{c\bar{r}\gamma}. \tag{24}$$

By substituting Eq. (22) into Eq. $(20)_2$ along with Eq. (12), one can obtain a simple relation to estimate the macro-hardness H_o as follows:

$$H_o = \kappa\sigma_{ref}\sqrt{c\omega}. \tag{25}$$

It can be noted that both Eqs. (23) and (25) in addition to $H = P/\pi a_p^2$ are functions of the residual contact radius, a_p. Therefore, Eq. (23) cannot be used alone to characterize the indentation size effect noticed in hardness experiments with spherical indenters. However, Lim and Choudhri [6] and Swadener et al. [9] have shown experimentally that for indentation of material with spherical indenters of few micron tip radii, the indentation hardness systematically increases with residual contact

radius a_p and decreases with the residual indentation profile diameter D_p. Lim and Choudhri [6] and Swadener et al. [9] tend to attribute the ISE to the different hardness values obtained for different spheres at the same value of the normalized contact radius $\omega = a_p/D_p$ (or equivalently at fixed effective plastic strain $\varepsilon^p = c\omega$). Therefore, by substituting $a_p = \omega D_p$ into Eq. (23), one obtains a relation that can characterize the ISE for a constant ω, such that:

$$\frac{H}{H_o} = 1 + \sqrt{\frac{D^*}{D_p}}, \tag{26}$$

where D^* is a material specific parameter that characterizes the size dependence of hardness and depends on the indenter geometry as well as on the plastic flow such that it is given by:

$$D^* = \xi \ell \text{ with } \xi = \frac{2}{c\bar{r}\gamma\omega}. \tag{27}$$

Eq. (27) shows that D^* is a linear function of the length scale parameter ℓ. Thus, D^* is a crucial material parameter that characterizes the indentation size effect and its accurate experimental measure using spherical indenters yields a reasonable value for the intrinsic material length scale parameter in the strain gradient plasticity theory.

By assuming that both SSDs and GNDs are coupled in a linear sense (i.e., $\rho_T = \rho_S + \rho_G$), Swadener et al. [9] proposed the following ISE model:

$$\frac{H}{H_o} = \sqrt{1 + \frac{D^*}{D_p}}. \tag{28}$$

Swadener et al.'s model is commonly used to predict the microhardness of metals. Therefore, it is interesting to compare the predictions from Swadener et al.'s model, Eq. (28), and the proposed model, Eq. (26).

It is noteworthy that the expression for γ in Eq. $(17)_2$ can be expressed in terms of ω by adapting the following relations between a_p, h_p, and D_p proposed by Kucharski and Mroz [40]:

$$a_p = \sqrt{q^2 D_p h_p} \quad \text{with} \quad q^2 = 2.5\left(\frac{2n-1}{4n+1}\right), \tag{29}$$

where q^2 is a constant that depends on the strain hardening exponent n and is mostly on the order of 1.0. Therefore, by substituting Eq. $(29)_1$ into Eq. $(17)_2$, one can rewrite the expression for γ in terms of $\omega = a_p/D_p$ as follows:

$$\gamma = 1 - \frac{3\omega}{4f^3q^2}. \tag{30}$$

Moreover, a value for the factor f in $c_p = fa_p$ can be inferred from the following well-established relation that is commonly used to calculate the size of the plastic zone under a spherical indenter [41]:

$$c_p = \sqrt{\frac{3P}{2\pi\sigma_y}}, \tag{31}$$

where P is the indentation load and σ_y is the yield strength. Substituting in the above expression $H = P/\pi a_p^2$, which is size-dependent, with $H_y = \kappa\sigma_y$ from Eq. $(19)_1$, and $c_p = fa_p$ yields

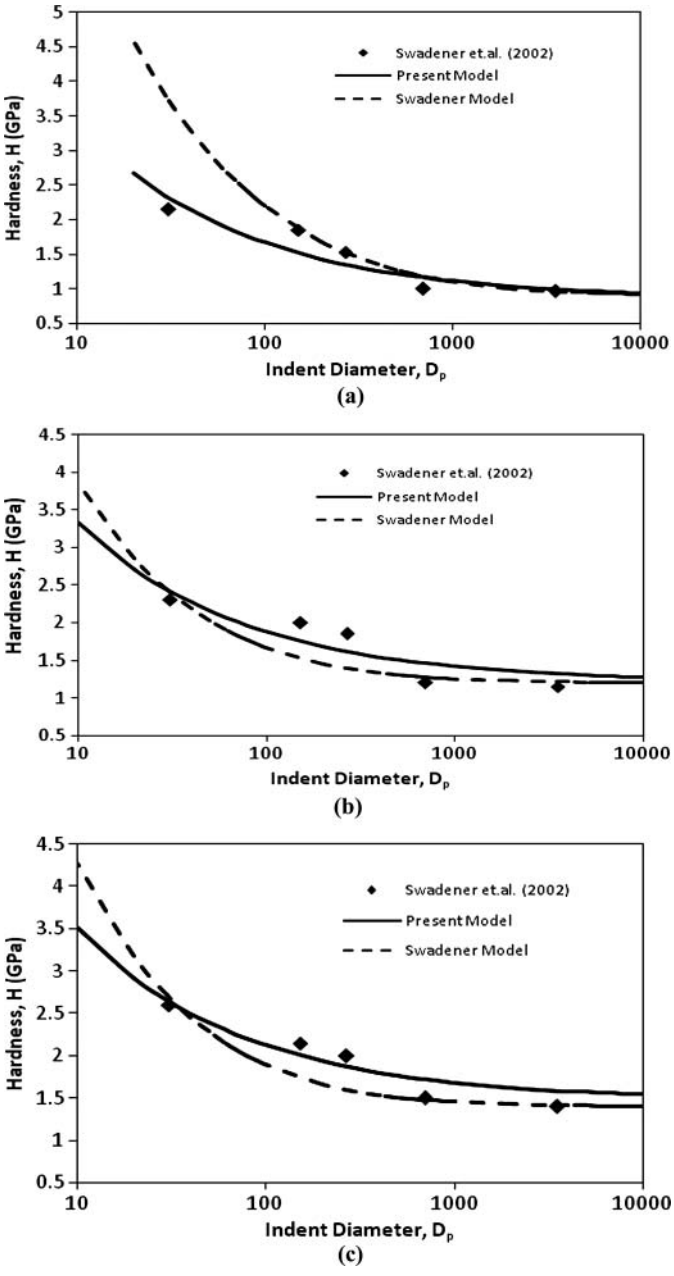

FIG. 2. Comparison of fit of the proposed model and Swadener et al.'s model to the experimental data on annealed iridium by Swadener et al. (2002) for (a) $\omega = 0.025$, (b) $\omega = 0.05$, and (c) $\omega = 0.075$.

$f = \sqrt{\frac{3}{2}\kappa H/H_y}$. However, $P/\pi c_p^2$ is observed experimentally to be roughly constant with respect to the indent size [42], which means that H is roughly constant at $r = c_p$. This suggests that the indentation hardness near the elastic-plastic boundary is already approximately self-similar and is not affected by size-dependent events at the indent core. It seems, therefore, that at $r = c_p$ one can set $H = H_y$, which gives the factor $f = \sqrt{\frac{3}{2}\kappa}$ such that f is constant. Substituting $\kappa = 3$ gives $f = 2.12$, which is in the range of the experimental values reported by Kramer et al. [43], Feng and Nix [21], and Durst et al. [29]. Then, note that if one assumes $f = 2.12$, $n = 2$, and $\omega = 0.05$, which are typical values for a metal, one obtains from Eq. (30) $\gamma \approx 1.0$. Therefore, $\gamma = 1.0$ will be assumed in the experimental comparisons in the following section.

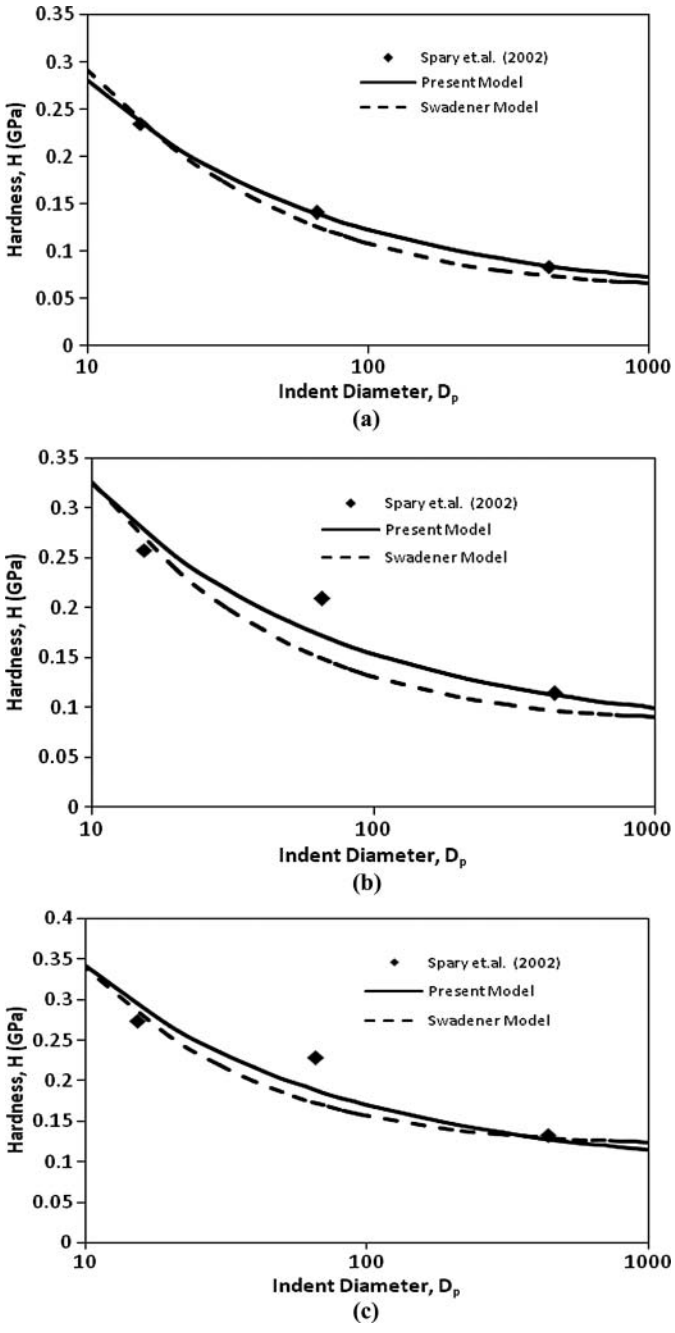

FIG. 3. Comparison of fit of the proposed model and Swadener et al.'s model to the experimental data on annealed aluminum by Spary et al. (2006) for (a) $\omega = 0.1$, (b) $\omega = 0.15$, and (c) $\omega = 0.2$.

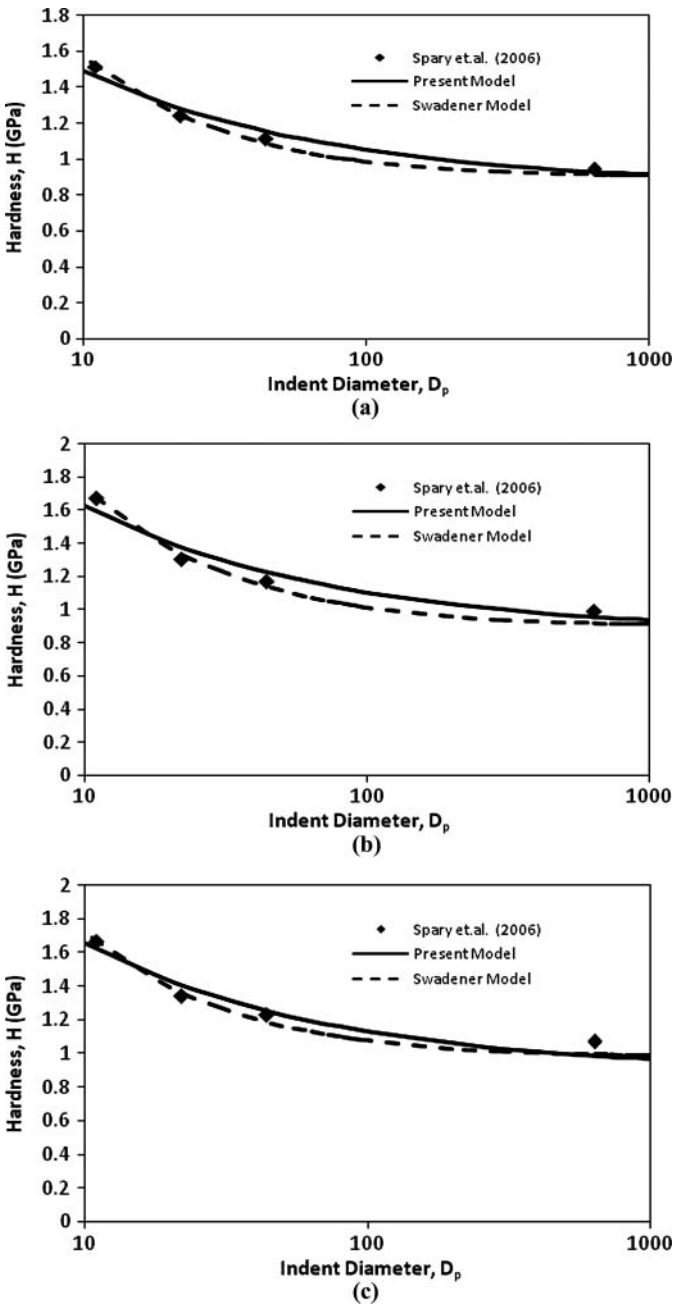

FIG. 4. Comparison of fit of the proposed model and Swadener et al.'s model to the experimental data on annealed nickel by Spary et al. (2006) for (a) $\omega = 0.05$, (b) $\omega = 0.1$, and (c) $\omega = 0.15$.

5. COMPARISON WITH EXPERIMENTAL DATA

In this section, comparisons are made between the predictions of the present ISE model in Eq. (26) and that of Swadener et al. [9] in Eq. (28) with several micro-indentation data from the literature. Unfortunately, nano-indentation data, i.e., for $D_p < 1\mu m$, could not be obtained from the reported indentation experiments in the literature. Therefore, nano-indentation data will be the focus of a future study in order to fully explore the ability of the proposed model and that of Swadener et al. [9] in predicting simultaneously micro- and nano-hardness indentation data. In fact, nano-indentation data using conical indenters are much more common in the literature as compared to that for spherical indenters. Detailed comparisons between the nano-indentation experimental data from conical indentation and the ISE's model for conical indenters that is established based on the proposed current approach are presented in Abu Al-Rub and Faruk [26]. In this study, the experimental data reported by Swadener et al. [9] on annealed iridium and by Spary et al. [44] on annealed aluminum and annealed nickel at different ratios of $\omega = a_p/D_p$ (or equivalently at different plastic strain levels) are utilized here to conduct this comparison for spherical indenters. All these materials have an FCC (face centered cubic) crystal microstructure. The values of D_p were not reported in these experiment, but is assumed here to be 1.1 D [9]. The experimental hardness data obtained from micro-indentations are plotted in Figures 2–4 as the hardness H versus the indentation diameter D_p at specific $\omega = a_p/D_p$ ratio. It can be seen from these figures that both the proposed model and Swadener et al.'s model fit well the micro-indentation hardness data. However, it can be seen that Swadener et al's model tends to overestimate the hardness data at low indentation depths (i.e., as the indentation depths are getting closer to the nano range). This is apparent in the fittings of annealed iridium data in Figure 2, where the present model fits well the hardness data at both high and low indentations, whereas Swadener et al.'s model overestimates the micro-hardness at low indentation diameters. Therefore, it will be interesting to compare the predictions of both models against nano-hardness data, which is the focus of a future study. Moreover, one can notice from the comparisons in Figures 2–4 that the ISE from the present model does not progressively vanish as fast as that of Swadener et al.'s model.

The characteristic form for the ISE presented by Eq. (26) gives a straight line when the hardness data are plotted as H/H_o versus $1/\sqrt{D_p}$, the intercept of which is 1.0 and the slope is $\sqrt{D^*}$. Taking a square of the slope of this curve gives the parameter D^* from which the material length scale ℓ can be calculated using Eq. (27). The macroscopic hardness H_o is obtained when the hardness curve reaches a plateau at large indentation depths. On the other hand, Swadener et al. [9] proposed plotting their model in Eq. (28) as $(H/H_o)^2$ versus $1/D_p$, which should result in a straight line with slope D^*. A summary of the fitting parameters H_o and D^* for specific ratios of contact radius to spherical indenter diameter, ω, is presented in Table 1. Also, the corresponding calculated values for the material length scale parameter ℓ are presented in Table 1. The dimensionless parameter ξ in Eq. $(27)_2$ is calculated by assuming that $c = 0.4$, the Nye factor $\bar{r} = 2$ [18], the plastic zone ratio $f = 2.12$ and $\gamma = 1$ as argued at the end of section 4, and ω as outlined in Table 1. The calculation of ℓ, therefore, strongly depends on the amount of plastic deformation as characterized by $\varepsilon^p = c\omega$. Generally, one can notice from the calculated values for ℓ in Table 1 that as ω increases ℓ decreases. Therefore, one can conclude that the material length scale is not fixed or constant for a specific material but depends on the course of deformation and should be considered as an internal variable. This agrees very well with the physical interpretation for ℓ as presented in Eq. $(10)_1$, which states that the material length scale in metals is related to the average spacing between dislocations or dislocations' mean free path. Indeed, as the level of plastic deformation increases, more dislocations are generated in the microstructure of the material, and the average spacing between dislocations decreases. Similar arguments have been presented in Abu Al-Rub and Voyiadjis [22, 31], Voyiadjis and Abu Al-Rub [34], Gomez and Basaran [24], and Abu Al-Rub [25], who stated that the length scale parameter is not fixed but decrease as the plastic strain increases. The results in Table 1 confirm their conclusion. Moreover, Abu

TABLE 1
The parameters of the present ISE model and the calculation of the length scale parameter ℓ from the fitted hardness data

Material	ω	H_0 (GPa)	D^* (μm)	ξ	$\ell = D^*/\xi$ (μm)
Ir	0.025	0.855 (0.9)*	90.827 (500)*	100.197	0.906
Ir	0.05	1.209 (1.2)	30.78 (93.05)	50.198	0.613
Ir	0.075	1.481 (1.4)	18.966 (83.11)	33.53	0.566
Al	0.10	0.075 (0.085)	110.67 (137.3)	25.198	4.392
Al	0.15	0.09 (0.12)	78.429 (69.93)	16.87	4.65
Al	0.20	0.11 (0.13)	48.414 (64.15)	12.699	3.812
Ni	0.05	0.85 (0.90)	5.693 (20.17)	50.198	0.113
Ni	0.10	0.86 (0.90)	7.998 (26.59)	25.198	0.317
Ni	0.15	0.89(0.98)	7.366(20.67)	16.87	0.437

*The values between brackets are from Swadener et al.'s model.

Al-Rub and Faruk [26] have shown that the value of ℓ strongly depends on the amount of prestraining, as for work hardened materials.

Moreover, it can be seen from the identified values of D^* in Table 1 that when using the present model for fitting the micro-indentation hardness data, smaller values for the material length scale parameter are identified than that obtained by the Swadener et al.'s model. Therefore, it can be concluded that Swadener et al.'s model overestimates the length scale parameter whereas the values from the present model are in the order of the spacing between dislocations, which is more physically sound as suggested by Eq. $(10)_1$.

6. CONCLUSIONS

In this article, a dislocation-based indentation size effect (ISE) model is formulated for micro- and nano-indentations when using a spherical indenter with different sizes. A fundamental difference between the formulation of the present ISE model and that of Swadener et al. [9] model is in the assumed coupling between the densities of SSDs and GNDs in the Taylor's hardening law for metals. In formulating the Swadener et al.'s ISE model a gross assumption is made such that the total dislocation density is a simple arithmetic sum of the densities of SSDs and GNDs, whereas in the current model a simple arithmetic sum of the Taylor's flow stresses from SSD and GND densities is found to be more appropriate. This fundamental difference resulted in a new ISE model which corrects the impediment of the Swadener et al.'s model in overestimating the nano-hardness data such that the present ISE model can fit better both the micro- and nano-hardness data simultaneously. Therefore, one may conclude that when using the Taylor's hardening law a simple sum of flow stresses from SSDs and GNDs is more adequate than the simple sum of SSD and GND densities.

Moreover, from dislocation-based arguments it is shown that the material length scale parameter in the strain gradient plasticity theory is not fixed or constant but changes with the course of plastic deformation such that it scales with the average spacing between dislocations. This conclusion is supported by calculating the material length scale parameter from the hardness data from spherical indentation at different plastic strain levels. Generally, it is shown that as the plastic strain level increases a smaller value for the material length scale is obtained. This suggested that the material length scale should be considered as an internal variable instead of a free parameter.

ACKNOWLEDGMENTS

The work reported in this article is supported by a joint grant from the U.S. National Science Foundation and the U.S. Department of Energy (NSF#0728032). Also, this research is supported by a grant from the U.S. Army Research Office (W911NF-09-1-0074). These supports are gratefully acknowledged.

REFERENCES

1. N.A. Stelmashenko, M.G. Walls, L.M. Brown, and Y.V. Milman, Microindentation on W and Mo oriented single crystals: An STM study. Acta Metallurg. Mater. vol. 41, pp. 2855–2865, 1993.
2. M.S. De Guzman, G. Neubauer, P. Flinn, and W.D. Nix, The role of indentation depth on the measured hardness of materials, Mater. Res. Symp. Proc., vol. 308, pp. 613–618, 1993.
3. Q. Ma and D.R. Clarke, Size dependent hardness in silver single crystals, J. Mater. Res., vol. 10, pp. 853–863, 1995.
4. W.J. Poole, M.F. Ashby, and N.A. Fleck, Micro-hardness of annealed and work-hardened copper polycrystals. Scripta Mater., vol. 34, pp. 559–564, 1996.
5. K.W. McElhaney, J.J. Valssak, and W.D. Nix, Determination of indenter tip geometry and indentation contact area for depth sensing indentation experiments, J. Mater. Res., vol. 13, pp. 1300–1306, 1998.
6. Y.Y. Lim and Y.Y. Chaudhri, The effect of the indenter load on the nanohardness of ductile metals: An experimental study of polycrystalline work-hardened and annealed oxygen-free copper, Philoso. Maga. A, vol. 79, no. 12, pp. 2979–3000, 1999.
7. A.A. Elmustafa and D.S. Stone, Indentation size effect in polycrystalline F.C.C metals, Acta Mater., vol. 50, pp. 3641–3650, 2002.
8. W.W. Gerberich, N.I. Tymiak, J.C. Grunlan, M.F. Horstemeyer, and M.I. Baskes, Interpretation of indentation size effects, ASME Trans., J. Appl. Mech., vol. 69, pp. 433–442, 2002.
9. J.G. Swadener, E.P. George, and G.M. Pharr, The correlation of the indentation size effect measured with indenters of various shapes, J. Mech. Phys. Solids, vol. 50, pp. 681–694, 2002.
10. D.J. Lloyd, Particle reinforced aluminum and magnesium matrix composites, Int. Mater. Rev., vol. 39, pp. 1–23, 1994.
11. C.-W. Nan and D.R. Clarke, The influence of particle size and particle fracture on the elastic/plastic deformation of metal matrix composites, Acta Mater., vol. 44, pp. 3801–3811, 1996.
12. M.T. Kiser, F.W. Zok, and D.S. Wilkinson, Plastic flow and fracture of a particulate metal matrix composite, Acta Mater., vol. 44, pp. 3465–3476, 1996.
13. J.S. Stolken and A.G. Evans, A microbend test method for measuring the plasticity length-scale, Acta Mater., vol. 46, pp. 5109–5115, 1998.
14. P. Shrotriya, S.M. Allameh, J. Lou, T. Buchheit, and W.O. Soboyejo, On the measurement of the plasticity length scale parameter in LIGA nickel foils, Mech. Mater., vol. 35, pp. 233–243, 2003.
15. M.A. Haque and M.T.A. Saif, Strain gradient effect in nanoscale thin films, Acta Mater., vol. 51, pp. 3053–3061, 2003.
16. G.Z. Voyiadjis and R.K. Abu Al-Rub, Nonlocal Continuum Damage and Plasticity: Theory and Computation. World Scientific Publishing Co Pte Ltd., UK, 2010.
17. M.F. Ashby, The deformation of plastically non-homogenous alloys, Philos. Maga., vol. 21, pp. 399–424, 1970.
18. A. Arsenlis and D.M. Parks, Crystallographic aspects of geometrically-necessary and statistically-stored dislocation density, Acta Mater., vol. 47, pp. 1597–1611, 1999.
19. W.D. Nix and H. Gao, Indentation size effects in crystalline materials: A law for strain gradient plasticity, J. Mech. Phys. Solids, vol. 46, pp. 411–425, 1998.
20. R. Saha, Z. Xue, Y. Huang, and W.D. Nix, Indentation of a soft metal film on a hard substrate: strain gradient hardening effects, J. Mech. Phys. Solids, vol. 49, pp. 1997–2014, 2001.
21. G. Feng and W.D. Nix, Indentation size effect in MgO, Scripta Mater., vol. 51, pp. 599–603, 2004.
22. R.K. Abu Al-Rub and G.Z. Voyiadjis, Analytical and experimental determination of the material intrinsic length scale of strain gradient plasticity theory from micro- and nano-indentation experiments, Int. J. Plastic., vol. 20, pp. 1139–1182, 2004.
23. I. Manika and J. Maniks, Size effects in micro- and nanoscale indentation, Acta Mater., vol. 54, pp. 2049–2056, 2006.

24. J. Gomez and C. Basaran, Nano-indentation of Pb/Sn solder alloys: Experimental and finite element simulation results, Int. J. Solids & Struc., vol. 43, pp. 1505–1527, 2006.
25. R.K. Abu Al-Rub, Prediction of micro and nanoindentation size effect from conical or pyramidal indentation, Mech. Mater., vol. 39, pp. 787–802, 2007.
26. R.K. Abu Al-Rub and A.N.M. Faruk, Dislocation-based model for predicting size-scale effects on the micro and nano indentation hardness of metallic materials, Int. J. Mater. Struc. Integ., vol. 4, nos. 2–4, pp. 251–277, 2010.
27. Y. Huang, F. Zhang, K.C. Hwang, W.D. Nix, G.M. Pharr, and G. Feng, A model of size effects in nano-indentation, J. Mech. Phys. Solids, vol. 54, pp. 1668–1686, 2006.
28. D. Chicot, Hardness length-scale factor to model nano- and micro-indentation size effects, Mater. Sci. Eng. A, vol. 499, nos. 1–2, pp. 454–461, 2009.
29. K. Durst, B. Backes, O. Franke, and M. Goken, Indentation size effect in metallic materials: Modeling strength from pop-in to macroscopic hardness using geometrically necessary dislocations, Acta Mater., vol. 54, pp. 2547–2555, 2006.
30. G.I. Taylor, Plastic strain in metals, J. Inst. Metals, vol. 62, pp. 307–324, 1938.
31. R.K. Abu Al-Rub and G.Z. Voyiadjis, Determination of the material intrinsic length scale of gradient plasticity theory, Int. J. Multiscale Comput. Eng., vol. 3, no. 3, pp. 50–74, 2004.
32. J.F. Nye, Some geometrical relations in dislocated crystals, Acta Metallurg., vol. 1, pp. 153–162, 1953.
33. H. Mughrabi, On the role of strain gradients and long-range internal stresses in the composite model of crystal plasticity, Mater. Sci. Eng. A, vol. 317, pp. 171–180, 2001.
34. G.Z. Voyiadjis and R.K. Abu Al-Rub, Gradient plasticity theory with a variable length scale parameter, Int. J. Solids & Struc., vol. 42, pp. 3998–4029, 2005.
35. E. Orowan, Discussion in Symposium on Internal Stresses in Metals and Alloys. Institute of Metals, London, p. 451, 1948.
36. M.R. Begley and M.R. Hutchinson, The mechanics of size-dependent indentation, J. Mech. Phys. Solids, vol. 46, pp. 2049–2068, 1998.
37. M. Zhao, W.S. Slaughter, M. Li, and S.X. Mao, Material-length-scale-controlled nanoindentation size effects due to strain-gradient plasticity, Acta Mater., vol. 51, pp. 4461–4469, 2003.
38. D. Tabor, The Hardness of Metals. Clarendon Press, Oxford, 1951.
39. A.G. Atkins and D.T. Tabor, Plastic indentation in metals with cones, J. Mech. Phys. Solids, vol. 13, pp. 149–164, 1965.
40. S. Kucharski and Z. Mroz, Identification of plastic hardening parameters of metals from spherical indentation tests, Mater. Sci. Eng. A, vol. 318, pp. 65–76, 2001.
41. K.L. Johnson, The correlation of indentation experiments, J. Mech. Phys. Solids, vol. 18, pp. 115–126, 1970.
42. Y.L. Chiu and A.H.W. Ngan, A TEM investigation on indentation plastic zones in Ni3Al(Cr,B) single crystals, Acta Mater., vol. 50, pp. 2677–2691, 2002.
43. D. Kramer, H. Huang, M. Kriese, J. Rohack, J. Nelson, A. Wright, D. Bahr, and W.W. Gerberich, Yield strength predictions from the plastic zone around nanocontacts. Acta Mater., vol. 47, pp. 333–343, 1999.
44. I.J. Spary, A.J. Bushby, and N.M. Jennett, On the indentation size effect in spherical indentation, Philosoph. Mag., vol. 86, pp. 5581–5593, 2006.